

# Chapter 2

## Methodology

### 2.1 Basic Background of Molecular Dynamics Simulation

Molecular dynamics simulation solves Newton's second law of motion for each atom  $\sum_j \mathbf{F}_{ij} = m_i \frac{d^2 \mathbf{r}_i}{dt^2}$ , where  $m_i$ ,  $\mathbf{r}_i$ ,  $t$ , and  $\mathbf{F}_{ij}$  are atomic mass, position of atom  $i$ , time, and force between atoms  $i$  and  $j$ , respectively. The equation of motion is usually integrated with the random initial configurations and initial velocities calculated from Boltzmann distribution [1]. Solving the equation of motion requires the input of atomic mass, time step, and force. While it is straightforward to provide atomic mass and time step (e.g., 1 fs) the determination of the force between atom  $i$  and  $j$  requires special care because MD simulation results strongly depend on the applied force field. The force  $\mathbf{F}$  is calculated from the interaction potential  $V_{ij}$  as  $\mathbf{F}_{ij} = -\nabla_i V_{ij}$ .

#### 2.1.1 Force Field

In my simulations, non-bonded potential energy is described as:

$$V_{ij} = 4\varepsilon_{ij} \left[ \left( \frac{\delta_{ij}}{r_{ij}} \right)^{12} - \left( \frac{\delta_{ij}}{r_{ij}} \right)^6 \right] + f \frac{q_i q_j}{\varepsilon_r r_{ij}} \quad (2.1)$$

The first terms in the right-hand side of Eq. (2.1) describe Lennard-Jones (LJ) interaction. The second terms in the right-hand side of Eq. (2.1) describe electrostatic potentials. The cross LJ interaction between unlike species is given by the Lorentz-Berthelot mixing rules:  $\sigma_{ij} = \frac{\sigma_{ii} + \sigma_{jj}}{2}$  and  $\varepsilon_{ij} = \sqrt{\varepsilon_{ii} \varepsilon_{jj}}$ . The calculation of the non-bonded interactions is the most time consuming step in molecular dynamics

simulation. To speed up the computation, the interactions between two atoms separated by a distance greater than the cutoff distance are ignored. While this approach works well for the Lennard-Jones interaction it is not suitable to implement for the system where charged atoms are present because of the significance of the long-range electrostatic interaction. The most popular method to approximate the electrostatic interaction is to partition it into a long-range component and a short-range component. The short-range component is calculated following Eq. (2.1) in real space and the long-range one is estimated in Fourier space using different approaches including Ewald, particle-mesh Ewald (PME), and Particle-Particle Particle-Mesh methods [1]. These methods require less computer time compared to the direct summation using Eq. (2.1). In my simulations I usually implement PME algorithm to calculate the long-range electrostatic interaction.

As water is present in all of my simulated systems selecting the good water model is critical to simulation results. There are a lot of models available in literature including SPC [2], SPC/E [3], TIP4P/2005 [4], TIP3P [5], TIP5P [6], TIP4P/2005f [7], and SWM4\_NDP [8] water models. SPC and SPC/E are the three sites rigid water models. Partial charges are assigned to oxygen and hydrogen atoms, while the center of LJ interactions is the oxygen atom. When the rigid SPC/E model is implemented, the two O–H bonds and the fictitious H–H bond lengths were constrained using the SHAKE algorithm [9]. TIP4P/2005 is a four sites rigid model. The oxygen atom carries no charge and is the center of LJ interaction. Partial charges are assigned to each hydrogen atom and to a dummy atom M located along the bisector of the HOH angle. TIP5P is a rigid five-sites water model. A partial charge is placed on each hydrogen atom, and partial charges of equal magnitude and opposite sign are placed on two lone-pair interaction sites. The oxygen atom has no charge and it functions as the center of LJ interactions. TIP3P is a three-sites rigid water model. It was developed to improve the energy and density for liquid water [5]. TIP4P/2005f is the flexible version TIP4P/2005 water model [7]. The O–H bond and HOH angle are allowed to vibrate in this water models. SWM4\_DP is a polarizable water model with four sites and Drude polarizability. The oxygen atom is the center of LJ interactions. The charge distribution is represented by three point charges: two hydrogen sites and one additional site positioned along the HOH bisector. Electronic induction is described by introducing a classical charged Drude particle attached to the oxygen by a harmonic spring. The oxygen atom carries a partial charge equal and opposite that of the Drude particle.

In my thesis, because I study the structural and dynamical properties of interfacial water the selected water model is expected to reproduce, at least the properties of bulk water. Mark and Nilsson [10], in the study of the structure and dynamics of the TIP3P, SPC, SPC/E water models at 297 K, compared the radial distribution function  $g_{OO}$ ,  $g_{OH}$ , and  $g_{HH}$  (i.e., a common property used to study structure of liquid water) and self-diffusion coefficients with experimental data. They reported that SPC/E model give the best bulk water dynamics and structure and SPC and TIP3P water models predict less water structure and faster diffusion when compared with experimental data. Pusztai et al. [11] compared the radial

**Table 2.1** Self-diffusion coefficients ( $10^{-5} \text{ cm}^2/\text{s}$ ) reported for some popular water models

H <sub>2</sub> O	SPC	SPC/E	TIP3P	TIP5P	TIP4P/2005	TIP4P/2005f	SWM4-NDP
D	3.85 [13]	2.49 [13]	5.13 [13]	2.62 [13]	2.08 [4]	1.93 [7]	2.33 [8]

distribution function of water models including SPC/E, TIP4P, TIP4P-2005 with the neutron diffraction data and reported that the structure of liquid water predicted using these water models are reasonable when compared with experimental data. For SWM4-NDP water model, while the radial distribution function  $g_{\text{OO}}$  is consistent with experimental data the  $g_{\text{OH}}$  and  $g_{\text{HH}}$  are slightly different from experimental results [8]. In the Table 2.1 I compare the self-diffusion coefficients reported for some popular water models. For comparison, the self-diffusion coefficient obtained from experiment is  $2.3 \times 10^{-5} \text{ cm}^2/\text{s}$  [12].

Among the popular water models mentioned SWM4-NDP reproduces the best experimental data of self-diffusion coefficient. While SPC, TIP3P, and TIP5P models overestimate TIP4P/2005 and TIP4P/2005f models underestimate the self-diffusion coefficient of water. Self-diffusion coefficient predicted using SPC/E model is slightly higher than experimental result.

A good water model is the model that reproduces all the properties of water molecules (e.g., dipole moment, dielectric constant, density, self-diffusion coefficient, radial distribution function, heat capacity, and phase diagram...). No water model in literature can reproduce all of these properties [14]. Because SPC/E is a simple (3 rigid sites) water model that reproduces well the experimental structure (i.e., radial distribution function  $g_{\text{OO}}$ ,  $g_{\text{OH}}$ , and  $g_{\text{HH}}$  [10]), and self-diffusion coefficient of water [13] at ambient conditions it is the model of choice in my simulation.

Molecular dynamics simulation results strongly depend on the force field describing the interactions among various constituents in the simulated system. For example, in one of my publications [15] I compare the water properties predicted on the crystalline silica substrate. I implement four different force fields to describe the silica surface. These force fields yield different orientation and flexibility of surface hydrogen atoms, and also different interaction potentials with water molecules. My results indicate the dependence of both structural and dynamical properties on the force field implemented. Comparison with experimental data is therefore necessary to discriminate the accuracy of implemented force fields. In this thesis, where this comparison is possible I will provide in details.

### 2.1.2 Algorithm

Solving the equation of motion requires the calculation of the pair-wise potential energy for all the atoms in the system. Due to the complicated nature of this

calculation, there is no analytical solution to the equations of motion. Therefore, a numerical method is applied. Numerous numerical algorithms have been developed to integrate the equations of motion including Verlet and leap-frog [1].

In my simulations I usually apply leap-frog algorithm to solve Newton's equations of motion. According to this algorithm, the position and velocity are described as follow:

$$r(t + \delta t) = r(t) + v(t + \frac{1}{2}\delta t)\delta t \quad (2.2)$$

$$v\left(t + \frac{1}{2}\delta t\right) = v\left(t - \frac{1}{2}\delta t\right) + \frac{F(t)}{m}\delta t \quad (2.3)$$

In Eq. (2.3) the velocities are calculated at time  $t + \frac{1}{2}\delta t$ . These are then used to calculate the positions  $r$  at time  $t + \delta t$ . In this way, the velocities leap over the positions, then the positions leap over the velocities. The velocities at time  $t$  can be approximated by Eq. (2.4):

$$v(t) = \frac{1}{2} \left[ v\left(t + \frac{1}{2}\delta t\right) + v\left(t - \frac{1}{2}\delta t\right) \right] \quad (2.4)$$

### 2.1.3 Thermostat

By simply solving the Newtonian equation of motion for all atoms in the system the NVE ensemble (i.e., microcanonical ensemble in which the number of atom, volume, energy are constant) is generated. Because molecular dynamics simulation results are expected to be compared with the experimental data, which are usually obtained at constant temperature, the NVT ensemble (i.e., canonical ensemble in which the number of atom, volume, temperature are constant) must be generated. Another reason I need to control the temperature, although it is not from the thermodynamic standpoint, is because of the numerical errors from MD simulation algorithm. Using thermostat can avoid steady energy drift from equilibrium state. Several thermostat methods are available in the literature including Andersen, Berendsen, Nose-Hoover [1]. For example, in Andersen thermostat the velocities of particles at each time step are reassigned the new values chosen from Maxwell-Boltzmann distribution [1, 16]. While this method requires no direct modification of the integration of equation of motion [16] it disturbs the velocity time correlations and slow down the kinetics of the system [1, 16]. Therefore, it should not be used to study dynamical properties. In Berendsen thermostat the deviation of the system temperature from target temperature  $T_0$  is corrected slowly as  $\frac{dT}{dt} = \frac{T_0 - T(t)}{\tau}$ , where  $\tau$  is the time constant. This approach does not yield a true canonical ensemble. However, when the system is large enough most of the

ensemble averages is not remarkably affected, except the kinetic energy distribution [1]. In the widely used Nose-Hoover thermostat the equation of motion is modified as:  $\frac{d^2 \mathbf{r}_i}{dt^2} = \frac{\mathbf{F}_i}{m_i} - \frac{p\zeta}{Q} \frac{d\mathbf{r}_i}{dt}$ . The friction parameter  $\zeta$  is a dynamic quantity and its equation of motion is described as:  $\frac{dp\zeta}{dt} = (T - T_0)$ . In my simulation I apply Noose-Hover thermostat because it allows one to rigorously generate a correct canonical ensemble [1].

Most of the equilibrium MD simulation results are quantified after equilibrium is established. To verify if the simulated system is equilibrated, temperature, structural and dynamical properties are monitored as a function of time. Equilibrium state is considered to be obtained when these properties do not change with simulation time.

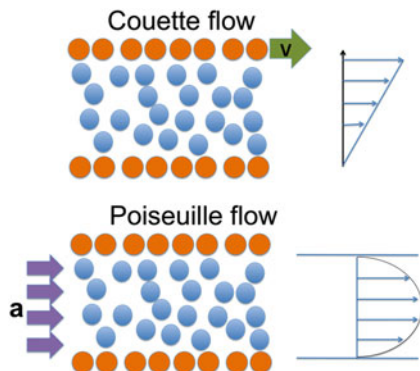
### 2.1.4 Periodic Boundary Condition

Periodic boundary conditions enable a large (infinite) system to be simulated using a small simulation box containing the atoms of interest. MD simulation algorithm is developed in a way that the central box is surrounded by its images in all directions. Atom in the central box interacts not only with the atoms in the same box but also with the atoms in the image box. In this way, the atoms in simulated box experience the forces as they are in large system. In my simulation I use cubic box and apply periodic boundary condition in all directions.

## 2.2 Non-equilibrium Simulation

In Fig. 2.1 I present two types of flow geometry implemented in this thesis to study the transport of fluids inside nanochannels. The first type is the Couette flow (top panel) [17], in which the atoms belonging to the top surface are driven at a constant

**Fig. 2.1** Schematic drawing showing the Couette (*top*) and Poiseuille (*bottom*) flow geometries used in my non-equilibrium simulations



velocity and the atoms belonging to the bottom surface are kept stationary. The typical velocity profile for this flow is shown in the top right panel. The second type is the Poiseuille flow (bottom panel), in which accelerations are applied to fluid atoms to force them to move in a specific direction [18]. The surfaces in Poiseuille flow geometry are kept stationary. The characteristic velocity profile of the Poiseuille flow is provided in bottom right panel. The non-equilibrium simulations are conducted until the velocity profile does not change with time (steady state flow).

In non-equilibrium MD simulations, the applied velocity in Couette geometry and the applied acceleration in Poiseuille flow are very large compared to those encountered in experiments. This is due to computing power limitations [18, 19]. However, because it has been reported that the time scale for fluid flow scales linearly with the applied acceleration [20, 21], and because many non-equilibrium MD simulation results are consistent with the experimental data [21, 22], I expect that reliable data can be obtained using non-equilibrium MD simulation.

Two approaches are usually used to control the temperature in non-equilibrium simulation: thermostat is coupled to all atoms in the system and thermostat is coupled only to the surfaces. In the later case, confined fluids exchange heat with the wall during the course of the simulation [23]. In my simulation I apply the former case. When implementing this algorithm it is essential to subtract the nonzero streaming velocity in the direction of the flow when calculating the kinetic energy. However, because the streaming velocity is un-known, only the velocity component perpendicular to the flow direction is usually thermostatted [24]. Since my streaming velocity is very small compared to the thermal velocity I include the streaming velocity in my temperature calculations. This will not result in significant error because small streaming velocity contributes only a tiny fraction of the total kinetic energy [25, 26]. Also, as demonstrated by Khare et al. [27], the differences in the temperature profiles expected at the shear rate considered in the this thesis are minimal and only present at the centre of the channel, the structure of interfacial water will not depend on the thermostat, and the conclusions in this thesis will hold independently on the algorithm considered.

The most common results presented in this thesis are the density and velocity profiles. In the left panel of Fig. 2.2 I show the schematic drawing presenting my

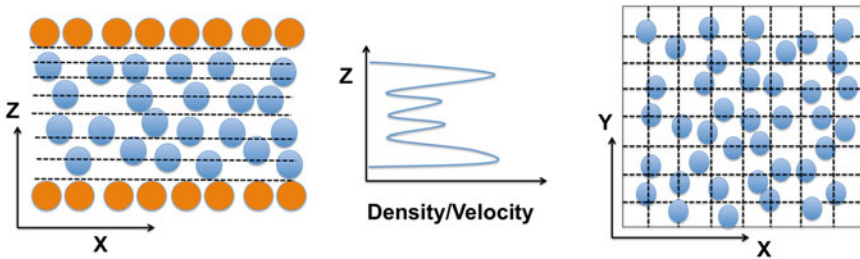


**Fig. 2.2** Schematic drawing showing the algorithm to calculate the profiles

algorithm to compute the velocity/density profiles as a functions of position in between two substrates. I divide the volume into bins that spans entire length of simulation box in X and Y directions, and 1 Å along the Z direction (dashed line). I then average the properties of the atoms in each bin over time. The averaged properties are plotted as a function of position z as shown in the middle panel. In the right panel of Fig. 2.2 I report the schematic drawing presenting my algorithm to calculate the planar density distribution, for example the distribution of water in the first hydration layer on the plane parallel to the surface. In this calculation, only the water in the layer of interest is taken into account. I divide the volume into small box of  $1 \times 1 \text{ Å}^2$  in XY plane and average the density inside each box over time. The density is then plotted in a 3D contour plot. For other properties reported in this thesis where the algorithm is applied I will provide in details.

## References

1. Van der Spoel, D., et al. (2005). GROMACS: Fast, flexible, and free. *Journal of Computational Chemistry*, 26(16), 1701–1718.
2. Berendsen, H. J. C., Postma, J. P. M., Van Gunsteren, W. F., & Hermans, J. (1981). *Intermolecular forces*. Dordrecht: Reidel.
3. Berendsen, H. J. C., Grigera, J. R., & Straatsma, T. P. (1987). The missing term in effective pair potentials. *Journal of Physical Chemistry*, 91(24), 6269–6271.
4. Abascal, J. L. F., & Vega, C. (2005). A general purpose model for the condensed phases of water: TIP4P/2005. *The Journal of Chemical Physics*, 123(23), 234505.
5. Jorgensen, W. L., Chandrasekhar, J., Madura, J. D., Impey, R. W., & Klein, M. L. (1983). Comparison of simple potential functions for simulating liquid water. *The Journal of Chemical Physics*, 79(2), 926–935.
6. Mahoney, M. W., & Jorgensen, W. L. (2000). A five-site model for liquid water and the reproduction of the density anomaly by rigid, nonpolarizable potential functions. *The Journal of Chemical Physics*, 112(20), 8910–8922.
7. Gonzalez, M. A., & Abascal, J. L. F. (2011). A flexible model for water based on TIP4P/2005. *The Journal of Chemical Physics*, 135(22), 224516–224523.
8. Lamoureux, G., Harder, E., Vorobyov, I. V., Roux, B., & MacKerell, A. D. (2006). A polarizable model of water for molecular dynamics simulations of biomolecules. *Chemical Physics Letters*, 418(1–3), 245–249.
9. Ryckaert, J.-P., Ciccotti, G., & Berendsen, H. (1977). Numerical integration of the cartesian equations of motion of a system with constraints: Molecular dynamics of n-alkanes. *Journal of Computational Physics*, 23(3), 327–341.
10. Mark, P., & Nilsson, L. (2001). Structure and dynamics of the TIP3P, SPC, and SPC/E water models at 298 K. *Journal of Physical Chemistry A*, 105(43), 9954–9960.
11. Pusztai, L., Pizio, O., & Sokolowski, S. (2008). Comparison of interaction potentials of liquid water with respect to their consistency with neutron diffraction data of pure heavy water. *The Journal of Chemical Physics*, 129(18), 184103.
12. Krynicki, K., Green, C. D., & Sawyer, D. W. (1978). Pressure and temperature-dependence of self-diffusion in water. *Faraday Discussions*, 66, 199–208.
13. Mahoney, M. W., & Jorgensen, W. L. (2001). Diffusion constant of the TIP5P model of liquid water. *The Journal of Chemical Physics*, 114(1), 363–366.
14. Vega, C., & Abascal, J. L. F. (2011). Simulating water with rigid non-polarizable models: A general perspective. *Physical Chemistry Chemical Physics: PCCP*, 13(44), 19663–19688.

15. Ho, T. A., et al. (2011). Interfacial water on crystalline silica: A comparative molecular dynamics simulation study. *Molecular Simulation*, 37(3), 172–195.
16. Basconi, J. E., & Shirts, M. R. (2013). Effects of temperature control algorithms on transport properties and kinetics in molecular dynamics simulations. *Journal of Chemical Theory and Computation*, 9(7), 2887–2899.
17. Thompson, P. A., & Troian, S. M. (1997). A general boundary condition for liquid flow at solid surfaces. *Nature*, 389(6649), 360.
18. Lauga, E., Brenner, M., & Stone, H. (2007). *Handbook of experimental fluid dynamics*. New York: Springer.
19. Ho, T. A., Papavassiliou, D. V., Lee, L. L., & Striolo, A. (2011). Liquid water can slip on a hydrophilic surface. *Proceedings of the National Academy of Sciences*, 108(39), 16170–16175.
20. Cohen-Tanugi, D., & Grossman, J. C. (2012). Water Desalination across nanoporous graphene. *Nano Letters*, 12(7), 3602–3608.
21. Holt, J. K., et al. (2006). Fast mass transport through sub-2-nanometer carbon nanotubes. *Science*, 312(5776), 1034–1037.
22. Whitby, M., & Quirke, N. (2007). Fluid flow in carbon nanotubes and nanopipes. *Nature Nanotechnology*, 2(2), 87–94.
23. Toton, D., Lorenz, C. D., Rompotis, N., Martsinovich, N., & Kantorovich, L. (2010). Temperature control in molecular dynamic simulations of non-equilibrium processes. *Journal of Physics: Condensed Matter*, 22(7), 074205.
24. Zhu, W., Singer, S. J., Zheng, Z., & Conlisk, A. T. (2005). Electro-osmotic flow of a model electrolyte. *Physical Review E*, 71(4), 041501.
25. Freund, J. B. (2002). Electro-osmosis in a nanometer-scale channel studied by atomistic simulation. *The Journal of Chemical Physics*, 116(5), 2194–2200.
26. Qiao, R., & Aluru, N. R. (2003). Ion concentrations and velocity profiles in nanochannel electroosmotic flows. *The Journal of Chemical Physics*, 118(10), 4692–4701.
27. Khare, R., de Pablo, J., & Yethiraj, A. (1997). Molecular simulation and continuum mechanics study of simple fluids in non-isothermal planar couette flows. *The Journal of Chemical Physics*, 107(7), 2589–2596.



Nanoscale Fluid Transport

From Molecular Signatures to Applications

Ho, T.A.

2017, XIV, 86 p. 31 illus., 25 illus. in color., Hardcover

ISBN: 978-3-319-47002-3